Visualization and Manipulation of Molecular Motion in Solid State through Photo-Induced Clusteroluminescence

Haoke Zhang[1,2#], Lili Du[3,4#], Lin Wang[5#], Junkai Liu[1,2], Qing Wan[6], Ryan T. K. Kwok[1,2], Jacky W. Y. Lam[1,2], David Lee Phillips[3*], and Ben Zhong Tang[1,2,6*]

[1]Department of Chemistry, Hong Kong Branch of Chinese National Engineering Research Center for Tissue Restoration and Reconstruction, The Hong Kong University of Science and Technology, Clear Water Bay, Kowloon, Hong Kong, China.

[2]HKUST-Shenzhen Research Institute, No. 9 Yuexing 1st RD, South Area, Hi-tech Park Nanshan, Shenzhen 518057, China

[3]Department of Chemistry, The University of Hong Kong, Pokfulam Road, Hong Kong, China

[4]Institute of Life Sciences, Jiangsu University, Zhenjiang 212013, China

[5]School of Biomedical Sciences, Faculty of Medicine, The Chinese University of Hong Kong, Shatin, NT, Hong Kong, China

[6]Center for Aggregation-Induced Emission, State Key Laboratory of Luminescent Materials and Devices, SCUT-HKUST Joint Research Institute, South China University of Technology, Tianhe Qu, Guangzhou 510640, China

These authors contributed equally: Haoke Zhang, Lili Du, Lin Wang.

Correspondence and requests for materials should be addressed to D.L.P. (email: phillips@hku.hk) or to B.Z.T. (email: tangbenz@ust.hk)

Abstract

Building molecular machine has long been a dream of scientists as it is expected to revolutionize many aspects of technology and medicine. Implementing the solid-state molecular motion is the prerequisite for a practical molecular machine. Study of it is not only scientifically important but also practically useful. However, currently few works on solid-state molecular motion have been reported as this process is hard to be manipulated. Meanwhile, it is almost impossible to “see” the motion even if it happens. Here we discover that non-conjugated molecules *s*-DPE and *s*-DPE-TM are capable to perform light-driven molecular motion in solid state, which results in the formation of excited-state though-space complex (ESTSC). Meanwhile, the newly formed ESTSC generates an abnormal visible emission which is termed as clusteroluminescence. Thus this photo-induced clusteroluminescence can be utilized to visualize the process of solid-state molecular motion. Notably, the original packing structure can be recovered from ESTSC when the light source is removed. Both the molecular motion process and formation of ESTSC have been confirmed by the time-resolved spectroscopy and quantum mechanics calculation. This work provides a new strategy to manipulate and “see” solid-state molecular motion and gains new insights into the mechanistic picture of clusteroluminescence.

Introduction

Everything in the world is ever-changing, and the change is the eternal truth of nature. All the macroscopic and microscopic changes can be traced back to molecular motion. The second law of thermodynamics states that the total entropy of an isolated system is always increased, which indicates the disordered nature of molecular motion[1]. It is noteworthy that most of the molecular motions are still random even with an external stimulus. In 2016, the Nobel Prize in chemistry was awarded to the “design and synthesis of molecular machines”. The typical feature of molecular machine is the unidirectional molecular motion which relies heavily on ingenious structural design[2-5]. Currently, molecules utilized as molecular machine are quite rare. In addition, from gas to liquid to solid states, the molecular motion becomes harder and harder. So almost all the mature molecular machines are only workable in the liquid state[6]. However, the promising applications of the molecular machine are in the solid state, such as cargos transportation and drug delivery[7,8]. Therefore, study of the solid-state molecular motion is the holy grail for a practical molecular machine, which is not only scientifically important but also practically useful[9,10].

Fundamentally, visualization of the solid-state molecular motion is beneficial to the creation of molecular machine. In previous studies, nuclear magnetic resonance (NMR)[11], X-ray powder diffraction (XRD)[12] and scanning tunneling microscope (STM)[13] et al. have been applied to characterize the molecular structures at different positions or states. Nonetheless, none of these methods can realize the in-situ, on-site and real-time visualization of solid-state molecular motion simultaneously. For example, NMR spectroscopy is only applicable in solution state and many of the structural information is lost in the solid-state NMR. Structural analysis based on XRD technique needs an extremely low temperature to freeze the molecular motion. STM can visualize the molecular motion in real time but only for single molecule. Samples in this condition cannot be regarded as the real solid state. Apart from the visualization, manipulation of the solid-state molecular motion is another important task. At present, the molecular motion can be driven by many stimuli such as light[14], pH[15], temperature[16] and electricity[17]. Due to the advantages of contactless spatial and temporal control and high frequencies, light is recognized as the best stimulus to trigger the molecular motion[18].

Fluorescence is a longer-wavelength emission from chromophores after absorbing the short-wavelength light[19]. Ideally, the light-driven molecular motion will lead to the change of emission intensity or wavelength as the fluorescence is conformationally dependent. According to these considerations, fluorescence is anticipated to be a good candidate to visualize the solid-state molecular motion. Traditionally, in order to enhance the fluorescence efficiency, molecules are designed with planar and rigid structures[20]. However, such structure will form a very compacted packing in the solid state which will restrict the molecular motion. At the same time, the strong intermolecular interaction will quench the solid-state emission and show aggregation-caused quenching (ACQ) effect[21]. Therefore, neither the solid-state molecular motion nor its visualization can be realized by traditional systems.

Aggregation-induced emission (AIE), as an opposite effect to ACQ, was proposed by Tang et al. in 2001[22,23]. Luminogens with AIE effect always show twist structures which will weaken the intermolecular interaction in their aggregate state. As a result, AIE luminogens (AIEgens) not only have strong emission but also a certain degree of mobility in the solid state[24,25]. That is the reason why the solid-state emission of AIEgens can be easily tuned by external stimuli, such as crystallization-induced emission and mechanochromism[26,27]. In particular, as a subgroup of AIEgens, clusteroluminogens are more sensitive to external stimuli than π-conjugated AIEgens[28].

Clusteroluminogens always show non-conjugated structures, such as polypeptide and sugar[29-31]. These molecules are nonluminescent in solution, but an abnormal visible emission is observed in the aggregate state which is termed as clusteroluminescence. Further studies reveal that this emission comes from through-space conjugation but not traditional through-bond conjugation. Notably, the non-conjugated structures endow the clusteroluminogens with higher structural mobility in the solid state than π-conjugated AIEgens[32]. In this work, we have designed two bibenzyl-based clusteroluminogens 1,2-diphenylethane (*s*-DPE) and 1,2-bis(2,4,5-trimethylphenyl)ethane (*s*-DPE-TM). In the solid state, these two structures proceed intermolecular motion after absorbing UV light, which results in the formation of excited-state though-space complexes (ESTSC). Meanwhile, clusteroluminescence is obtained in ESTSC which benefits from the strong intermolecular though-space conjugation. The ESTSC will automatically recover to its original irregular structures once the irradiation is removed (Fig. 1A). Our designed system easily realizes the light-driven intermolecular motion in solid state, and the in-situ, on-site and real-time visualization of this process is implemented by clusteroluminescence.

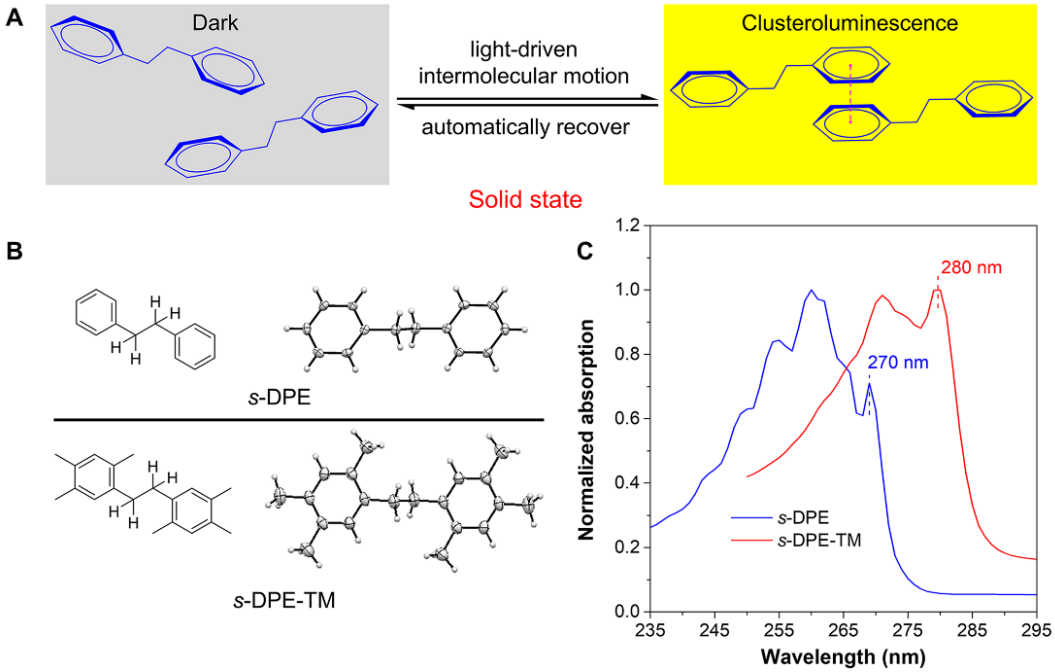

Fig. 1 (A) Schematic illustration of the light-driven intermolecular motion in solid state of *s*-DPE. (B) Crystal structures of *s*-DPE and *s*-DPE-TM. (C) Normalized absorption spectra of *s*-DPE and *s*-DPE-TM in acetonitrile solution.

Results and Discussion

Photo-induced clusteroluminescence. *s*-DPE and *s*-DPE-TM were synthesized according to the routes in Scheme S1. At first, it is expected that the *transoid*- and *cisoid*-*s*-DPE can be obtained from the hydrogenation of *trans*- and *cis*-stilbene, respectively. However, the structural characterization results illustrate that these two reactions produce the same compound *transoid*-*s*-DPE. Structures of *s*-DPE and *s*-DPE-TM were confirmed by NMR, high-resolution mass spectrometry (HRMS) and XRD (Fig. S1-8 and Fig. 1B, CCDC numbers: *s*-DPE ⊂ 1564142, *s*-DPE-TM ⊂ 1481601). UV absorption spectra in acetonitrile solution show that the absorption maximum of *s*-DPE and *s*-DPE-TM located at 280 and 270 nm which was the same with benzene and mesitylene, respectively[33]. So, Fig. 1C proves the non-conjugated nature of these two molecules. As expected, their photoluminescence (PL) spectra in pure tetrahydrofuran (THF) revealed that the emission maximum of *s*-DPE and

s-DPE-TM was 285 and 297 nm which was consistent with the absorption results. Fig. 2A and B show the emission behavior of *s*-DPE in its THF/water mixtures with different water faction (f_w). Previous studies tell that *s*-DPE will form aggregates at high f_w as water is the poor solvent.[34] When the f_w was lower than 60%, the 285 nm emission intensity (I) increased with the increase of f_w which was attributed to the polarity effect[33]. However, the intensity started to decrease once the f_w was bigger than 60%. Meanwhile, another longer-wavelength emission appeared around 355 nm at $f_w \geq 80\%$ which showed typical AIE effect. Similar results were observed in *s*-DPE-TM which had a new peak around 390 nm in aggregate state (Fig. 2C &D).

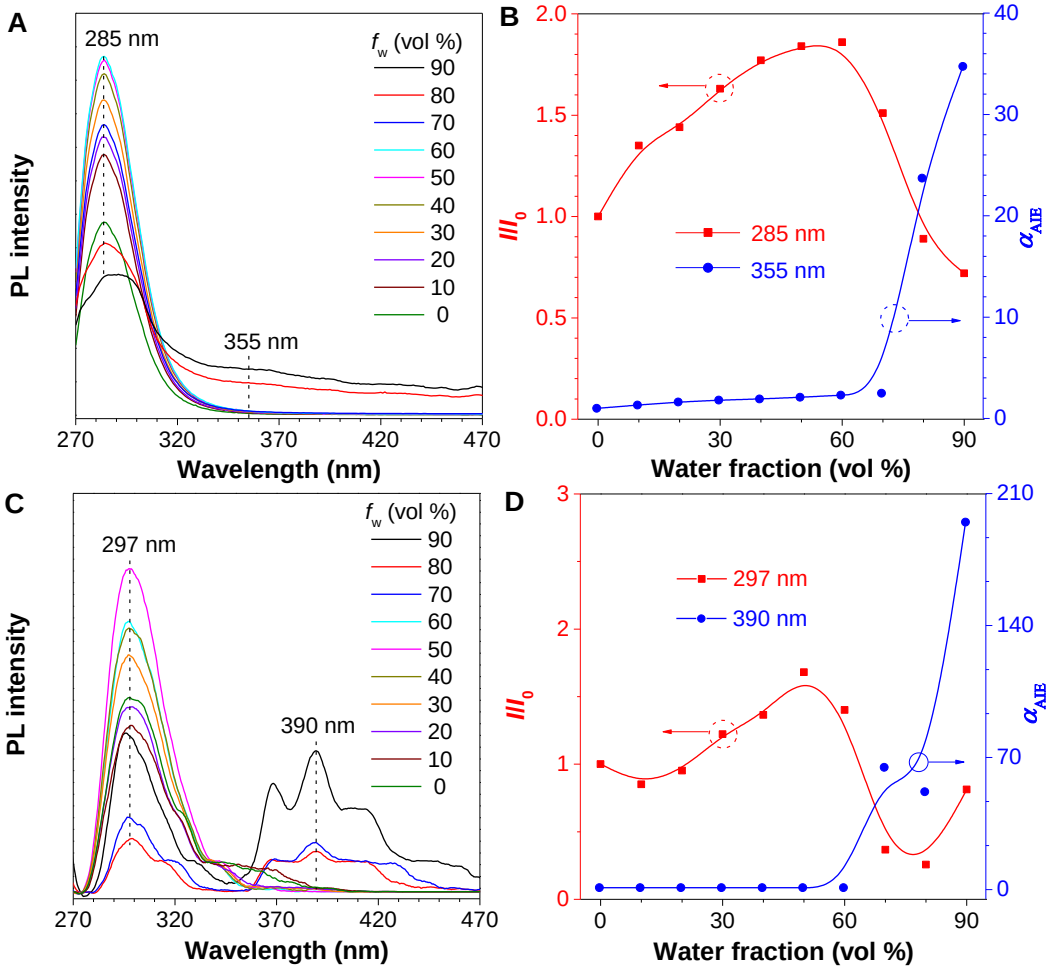

Fig. 2 Photoluminescence (PL) spectra of (A) *s*-DPE and (C) *s*-DPE-TM in THF/water mixture with different water fractions (f_w). Plots of relative PL intensity (I/I_0) versus f_w for (B) *s*-DPE and (D) *s*-DPE-TM. Concentration: 10^{-4} M, λ_{ex} = 260 nm for *s*-DPE and 280 nm for *s*-DPE-TM, I_0: intensity at f_w = 0%, $\alpha_{AIE} = I/I_0$ for the clusteroluminescence.

The solid-state PL spectra of *s*-DPE and *s*-DPE-TM also show two emission peaks at the same wavelength with their aggregate state (Fig. 3A). However, there are only benzene and mesitylene absorption peaks in their solid-state UV spectra (Fig. 3B). It is noteworthy that the emission intensity ratio of two peaks in *s*-DPE and *s*-DPE-TM show a big difference, for example, the I_{390}/I_{297} is only 3 for *s*-DPE-TM but the I_{355}/I_{285} reaches up 26 in *s*-DPE. This effect will be further discussed hereinafter. Aggregation-induced dual-emission effect has been reported in our previous tetraarylethane systems[33]. In that work, we termed the abnormal longer-wavelength emission as clusteroluminescence which was caused by the intramolecular through-space conjugation among four aryl rings. However, computational calculation on the monomer of *s*-DPE and *s*-DPE-TM reveals that no intramolecular

through-space conjugation was detected in these two molecules (Table S1). Meanwhile, the scanning potential energy surfaces of *s*-DPE also excluded the possibility of photoisomerization as large energy barriers existed in both the ground and excited states (Fig. S9). So, where does the clusteroluminescence of *s*-DPE and *s*-DPE-TM come from?

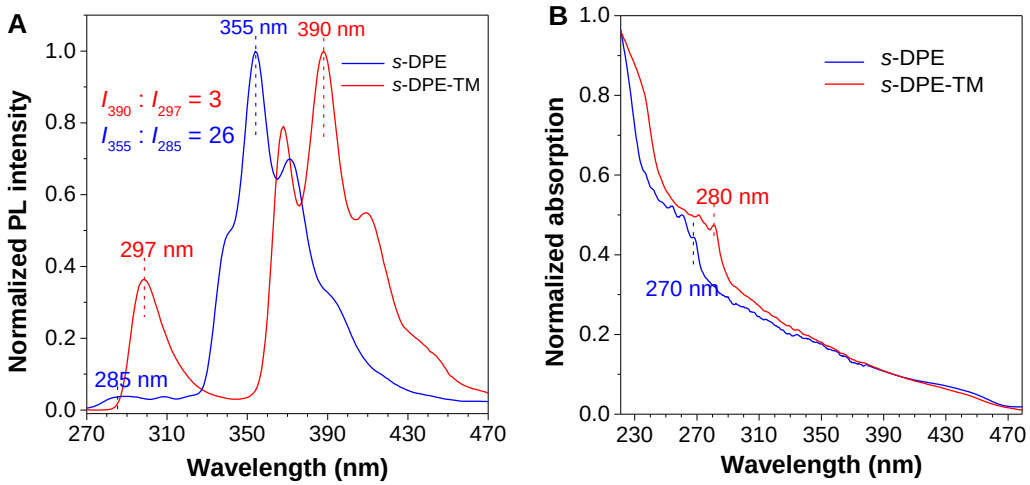

Fig. 3 Normalized (A) PL and (B) absorption spectra of *s*-DPE and *s*-DPE-TM in the solid state. λ_{ex} = 260 nm.

Steady-state photophysical studies suggest that the emitting species for clusteroluminescence only exist in excited state and the intramolecular though-space conjugation is excluded from the working mechanism. So, how about the intermolecular interaction[34]? Fortunately, single crystals of these two molecules have been obtained from their THF solution evaporation and the crystal structures were analyzed. As shown in Fig. S10 and 11, packing structures of *s*-DPE and *s*-DPE-TM indicate no strong intermolecular interaction in their dimer structures, which was further proved by ground-state dimer calculation (Table S1). The ground-state excitation energy (*E*) of dimer is similar to the monomer. For example, in *s*-DPE, the values of *E* are 5.49 and 5.51 eV for dimer and monomer, respectively. The ground-state simulation results are in good agreement with the absorption spectra. After that, the dimer structures were further optimized in excited state using the ωB97XD method with 6-311G* basis set[35]. The dimer structures both in ground and excited state can be found in Table S2-5.

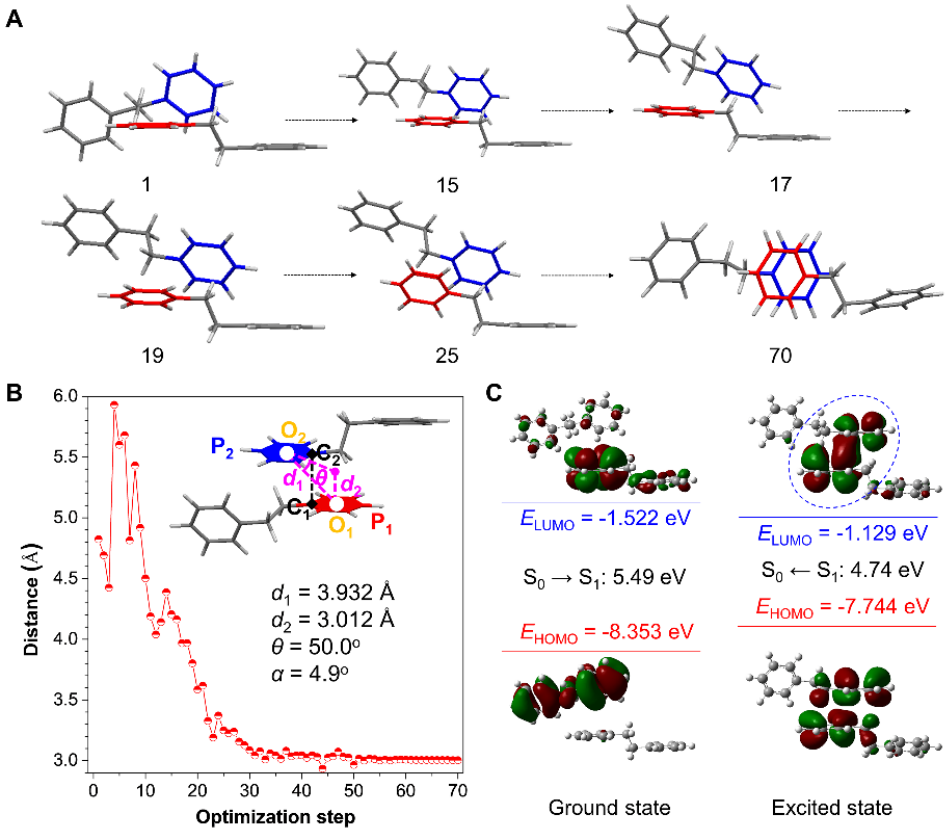

Fig. 4 (A) Conformational change of *s*-DPE dimer within the process of excited-state structural optimization, different numbers are different optimization steps. (B) Plot of atoms C1-C2 distance versus different optimization steps, inset: excited-state though-space complexes structure of *s*-DPE. P_1 and P_2: planes of phenyl ring, O_1 and O_2: centroids of phenyl ring, d_1: distance between O_1 and O_2, d_2: vertical distance between O_1 and P_2, θ: sin $\theta = d_2/d_1$, α: the angle between P_1 and P_2. (C) Frontier molecular orbitals of *s*-DPE-TM dimer both in the ground and excited states. E_{HOMO}: energy level of the Highest Occupied Molecular Orbital, E_{LUMO}: energy level of the Lowest Unoccupied Molecular Orbital, S_0: ground state, S_1: first excited state.

Quantum mechanics calculation. The structural variation of *s*-DPE within the process of excited-state optimization is shown in Fig. 4A. An obvious intermolecular motion and the formation of ESTSC are observed. Fig. 4B suggests that the two monomers moved close to each other as the distance between atoms C1 and C2 decreased from 6 to 3 Å. Inset in Fig. 4B illustrates the ESTSC structure of *s*-DPE. Fig. 4C shows that the *E* of ESTSC decreased to 4.74 eV along with the energy increase of highest occupied molecular orbital (HOMO) and decrease of lowest unoccupied molecular orbital (LUMO). Meanwhile, a strong intermolecular electronic coupling and though-space conjugation were observed in ESTSC but absent in the ground state. The same results were also collected for *s*-DPE-TM (Fig. 5A-C), which are in accordance with *s*-DPE. Intermolecular motion occurred in the process of excited-state dimer optimization and ESTSC was formed as its stable structure. Similarly, the *E* of ESTSC decreased to 4.59 eV which was 0.78 eV smaller than that in the ground state and a strong intermolecular electronic coupling was found in the ESTSC of *s*-DPE-TM.

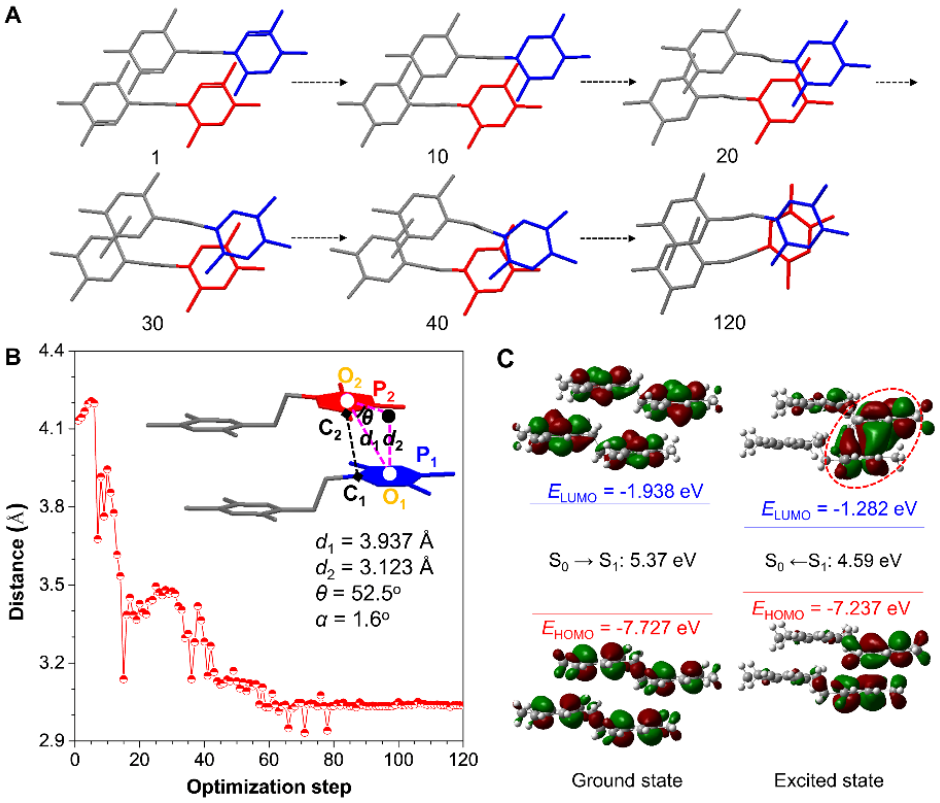

Fig. 5 (A) Conformational change of *s*-DPE-TM dimer within the process of excited-state structural optimization. (B) Plot of atoms C1-C2 distance versus different optimization steps, inset: excited-state though-space complexes structure of *s*-DPE-TM. (C) Frontier molecular orbitals of *s*-DPE-TM dimer both in the ground and excited states. P_1 and P_2: planes of phenyl ring, O_1 and O_2: centroids of phenyl ring, d_1: distance between O_1 and O_2, d_2: vertical distance between O_1 and P_2, θ: sin $\theta = d_2/d_1$, α: the angle between P_1 and P_2.

Time-resolved spectroscopy. Theoretically calculated data clearly demonstrate the process of intermolecular motion in solid state and the formation of ESTSC which is the luminous source of clusteroluminescence. However, there is still no experimental evidence to confirm the existence of light-driven intermolecular motion and ESTSC. Femtosecond transient absorption (fs-TA) spectroscopy is a widely used technique to study the excited-state properties such as photoreaction and other photo-induced processes[36-38]. So, is it possible to capture the process of ESTSC formation by fs-TA? Firstly, the transient absorption spectra were recorded for *s*-DPE and *s*-DPE-TM in their good solvents (Fig. S12&13). As expected, obvious transitions of $S_1 \rightarrow S_n$ located around 340 and 350 nm were observed for *s*-DPE and *s*-DPE-TM, respectively, Meanwhile, a shoulder peak around 450 nm was also found in these two molecules. Previous studies indicate that these short-wavelength peaks are assigned to the isolated units of benzene and trimethylbenzene[39,40], which serves as the evidence for the absence of ESTSC in solution.

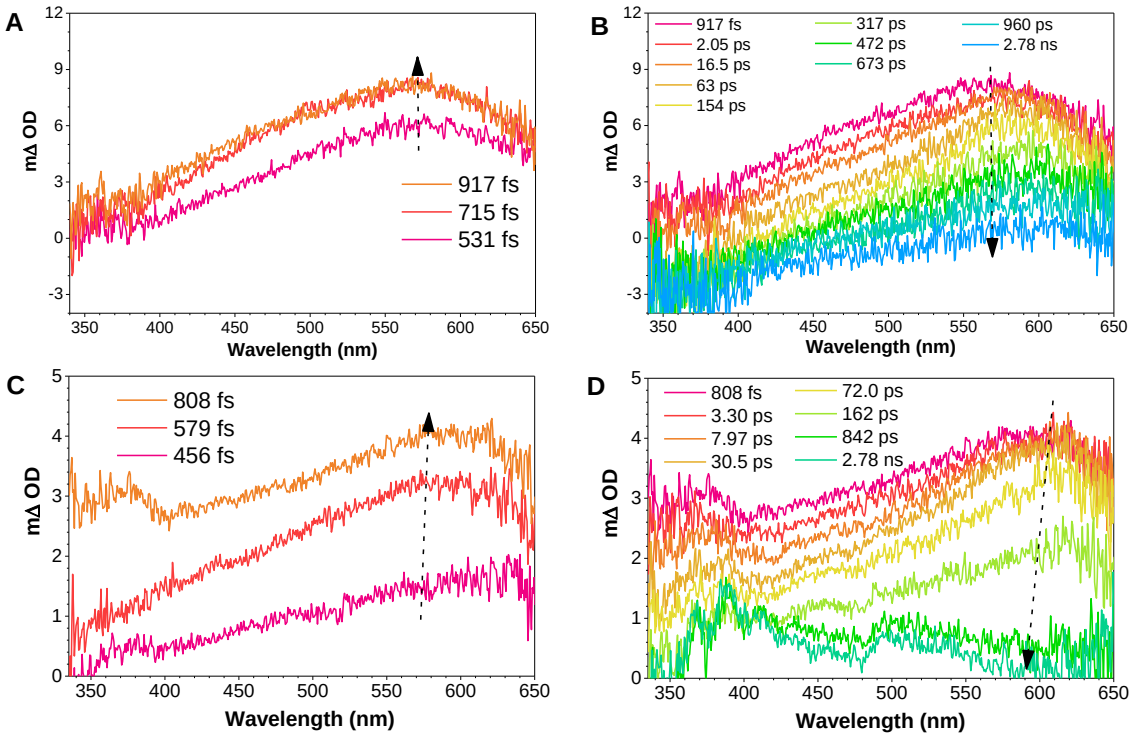

Fig. 6 (A) and (B): Femtosecond transient absorption (fs-TA) spectra of *s*-DPE in the film state with 267 nm excitation. (C) and (D): fs-TA spectra of *s*-DPE-TM in the film state with 267 nm excitation.

The fs-TA measurements were also conducted in the film state. As shown in Fig. 6A and B, the short-wavelength peaks around 340 and 450 nm almost disappeared and new peaks around 590 nm arose in *s*-DPE. According to the previous researches on benzene system, transitions around 590 nm is attributed to the excimer formation instead of the monomer itself[41,42]. The corresponding kinetic trace at 590 nm was shown in Fig. S14. It concludes that the broad peak at 590 nm is generated by the $S_1 \rightarrow S_n$ transition in ESTSC. The intensity of this peak decayed along with time from 917 fs to 2.78 ns and this process is repeatable, which indicates that the ESTSC will be automatically split once the light source is removed (Fig. 1A). A new peak around 615 nm was observed in *s*-DPE-TM in its film state (Fig. 6C and D, Fig. S15). Similarly, this peak is belonging to $S_1 \rightarrow S_n$ transition of ESTSC. It is noteworthy that, different from *s*-DPE, high-energy transition around 350 nm still exists in *s*-DPE-TM. At 2.78 ns, the corresponding fs-TA spectrum is similar to that in solution. Looking back to the solid-state PL spectra of *s*-DPE and *s*-DPE-TM, it was mentioned that the ESTSC/monomer ratio in *s*-DPE-TM was higher than *s*-DPE. In combining with fs-TA results, it concludes that the formation of ESTSC in *s*-DPE-TM is more difficult than that in *s*-DPE which should be ascribed to the strong intermolecular steric hindrance caused by the six methyl groups in *s*-DPE-TM.

Traditionally, fluorescent intensity and lifetime of a chromophore will decrease with the increase of its ambient temperature[43-45]. This is because the increased temperature will accelerate the molecular motion and enhance the nonradiative decay. However, in ESTSC, its clusteroluminescence is generated by molecular motion. In other words, the activation energy for solid-state intermolecular motion will decrease with the increase of temperature. As a result, different from traditional chromophores, the emission intensity of clusteroluminogens will be strengthened when increasing the temperature. As expected, the fluorescent intensity of *s*-DPE and *s*-DPE-TM decreased when the temperature was decreased from room temperature to 77 K (Fig. 7A & B). Meanwhile, the decay curves of clusteroluminescence from ESTSC were also recorded for these two molecules at different temperature (Fig. 7C,

Fig. S16). Surprisingly, in *s*-DPE-TM, its fluorescence lifetime (τ) continued to rise slowly from 7.2 to 8.5 ns with the temperature increasing from 77 to 298 K, which is similar to the behavior of thermally activated delayed fluorescence materials but with different mechanisms[46-50]. The increase of I and τ along with the increase of temperature further proves that the clusteroluminescence of ESTSC is resulted from solid-state molecular motion.

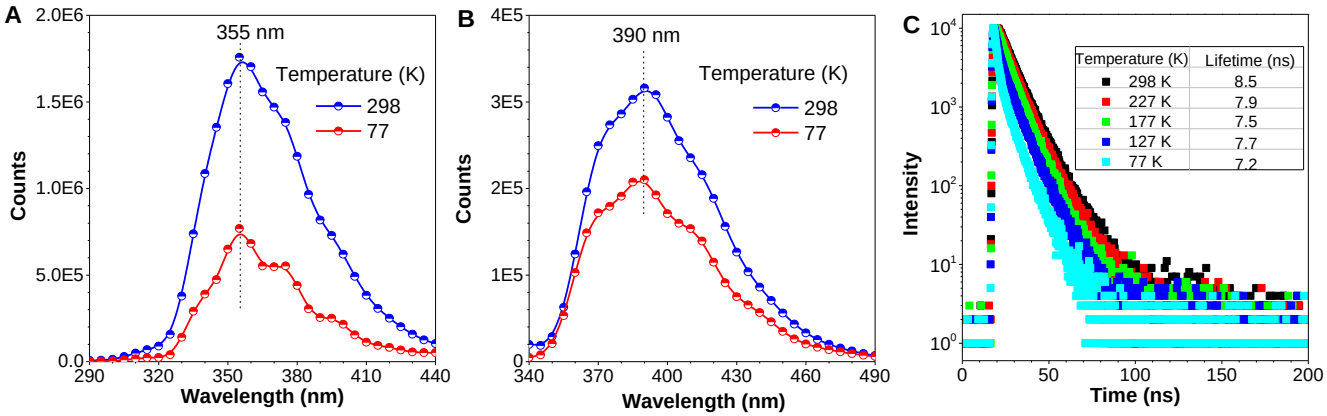

Fig. 7 PL spectra of (A) *s*-DPE and (B) *s*-DPE-TM in the solid state with the temperature increasing from 77 to 298 K. (C) Fluorescence decay curves of *s*-DPE-TM at 390 nm in the film state under different temperature.

So far, the ESTSC formed by solid-state intermolecular motion has been confirmed by both computational and experimental characterization. The photophysical picture of this process seems quite clear. However, it is significant to clarify the driving force for the light-driven intermolecular motion. Apparently, *s*-DPE and *s*-DPE-TM are two nonpolar hydrocarbon systems and their crystal structures suggest that there is no strong intermolecular interaction between two monomers. Then, partial atomic charges (δ) of these two molecules were mapped based on Mulliken population analysis (Fig. 8, Table S6&7). As shown in Fig. 8A, atoms C1 and C1' show positive δ (δ^+) as their outermost four electrons are all bonding with other three carbons. But the other carbons exhibit negative δ (δ^-) because all of them have one or two outermost electrons bonded with hydrogen. It is proposed that the opposite δ among these carbons will generate an intramolecular micro electric field. When two of the monomers are excited, driven by the interaction between their electric fields, they will get close to each other and form ESTSC. Fig. 8B indicates that the δ of C1 and C1' become more positive in ESTSC than that in the isolated monomer. Similarly, Mulliken population analysis on *s*-DPE-TM showed similar results with *s*-DPE (Fig. 8 C&D). In *s*-DPE-TM, there are eight carbons show δ^- which suggests a stronger intramolecular micro electric field than *s*-DPE. That is the reason why the ESTSC can still be formed even strong intermolecular steric hindrance exists in *s*-DPE-TM. In addition to the micro electric field, the London dispersion force is also believed to play an important role in driving the solid-state molecular motion[51,52].

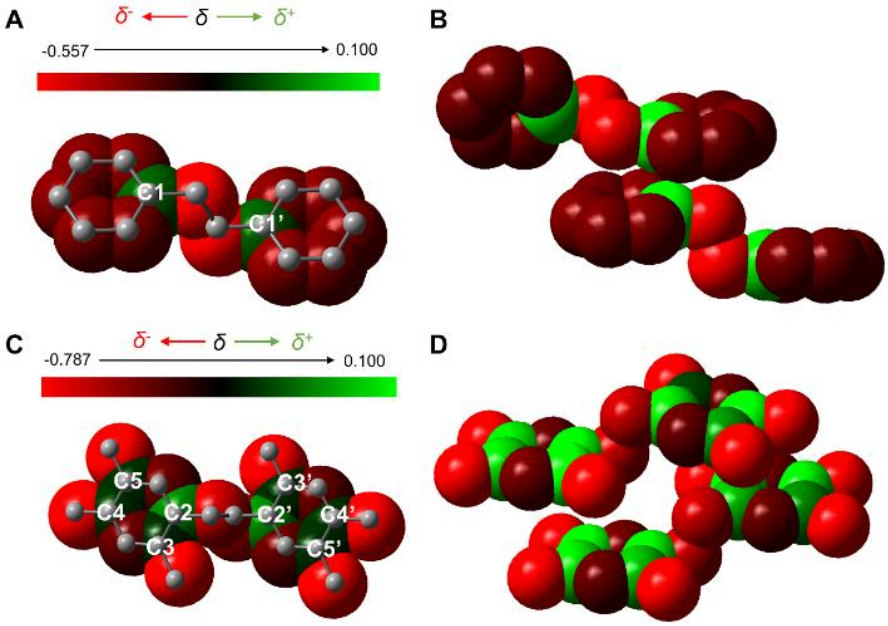

Fig. 8. Mulliken population analysis of *s*-DPE (A) monomer and (B) ESTSC, partial charge (*δ*) range: -0.557 to 0.100. *s*-DPE-TM (C) monomer and (D) ESTSC, *δ*: -0.787 to 0.100.

Conclusion

In summary, light-driven intermolecular motion in solid state occurs in two non-conjugated structures *s*-DPE and *s*-DPE-TM, which results in the formation of ESTSC. Experimentally, steady-state PL spectra show that these two molecules are AIE active and clusteroluminescence is observed in their aggregate state. Time-resolved absorption and emission spectra reveal that the clusteroluminescence of *s*-DPE and *s*-DPE-TM stems from their ESTSC. Quantum mechanics calculation further confirms the process of solid-state intermolecular motion and the formation of ESTSC. These results suggest that the solid-state intermolecular motion in *s*-DPE and *s*-DPE-TM can be manipulated by light and the original packing structure is recoverable when the light source is removed. In addition, the solid-state intermolecular motion is directly and simply visualized by clusteroluminescence. This work not only brings new ideas to design molecules with remarkable solid-state molecular motion but also develops an advanced method to “see” this invisible process and study the mechanistic picture of clusteroluminescence.

Methods

Femtosecond Transient Absorption Spectroscopy (fs-TA) measurement. The fs-TA measurements were performed based on a femtosecond Ti:Sapphire regenerative amplified laser system (Spectra Physics, Spitfire-Pro) and an automated data acquisition system (Ultrafast Systems, Helios model). The amplifier was seeded with the 120 fs output from the oscillator (Spectra Physics, Maitai). The probe pulse was obtained by using approximately 5% of the amplified 800 nm output from the Spitfire to generate a white-light continuum (325-650 nm) in a CaF2 crystal and then this probe beam was split into two parts before traversing the sample. One probe laser beam goes through the sample while the other probe laser beam goes to the reference spectrometer in order to monitor the fluctuations in the probe beam intensity. For the present experiments, the compounds *s*-DPE and *s*-DPE-TM in THF solution and thin film were excited by a 267 nm pump beam (the third harmonic of the fundamental 800 nm

from the regenerative amplifier). Samples of 1 mL solutions were studied in 2 mm path-length cuvette with an absorbance of 0.5 at 267 nm throughout the data acquisition. The thin films were prepared from their 1,2-dichloroethane solution by spin coating method.

Time-resolved fluorescence spectroscopy measurement. Lifetime and temperature dependent photoluminescence were measured on an Edinburgh FLSP 920 fluorescence spectrophotometer equipped with a xenon arc lamp (Xe900), a microsecond flash-lamp (uF900), a picosecond pulsed diode laser (EPL-375), a closed cycle cryostate (CS202*I-DMX-1SS, Advanced Research Systems) and an integrating sphere with nitrogen atmosphere. The solid-state sample was cooled down to 77 K and the first data were collected. Then, the temperature was gradually increased to room temperature and the other data were recorded at each set-point temperature.

Data availability

The authors declare that the data supporting the findings of this study are available within the article and its Supplementary Information files. Additional data are available from the corresponding author upon reasonable request.

Acknowledgments

We are grateful for financial support from the National Science Foundation of China (21788102), the Research Grants Council of Hong Kong (16308016, C6009-17G and A-HKUST 605/16), the University Grants Committee of Hong Kong (AoE/P-03/08 and AoE/P-02/12), the Innovation and Technology Commission (ITC-CNERC14SC01 and ITS/254/17) and the Science and Technology Plan of Shenzhen (JCYJ20160229205601482 and JCY20170818113602462).

Author contributions

H.Z. and B.T. designed the experiments. H.Z. synthesized all the compounds and measured all the PL, UV, QY, NMR, MS and XRD measurement. H.Z. and J.L. carried out the theoretical calculation and result analysis. L.D., Q.W. and D.L.P. did the time-resolved spectroscopy measurements. H.Z., J.W.Y.L. and R.T.K.K. discussed and proposed the mechanistic picture. H.Z. and L.W. revised the manuscript. H.Z. and B.T. wrote the manuscript with comments from all authors.

Additional information

Supplementary information and chemical compound information are available in the online version of the paper.

Competing interests: The authors declare no competing interests.

References

1. https://en.wikipedia.org/wiki/Second_law_of_thermodynamics.
2. Franken, L. E. et al. Solvent Mixing To Induce Molecular Motor Aggregation into Bowl-Shaped Particles: Underlying Mechanism, Particle Nature, and Application To Control Motor Behavior. *J. Am. Chem. Soc.* **140**, 7860–7868 (2018).

3. Roke, D., Stuckhardt, C., Danowski, W., Wezenberg, S. J. & Feringa, B. Light-Gated Rotation in a Molecular Motor Functionalized with a Dithienylethene Switch. *Angew. Chem. Int. Ed.* **57**, 10515-10519 (2018).
4. Roke, D., Wezenberg, S. J. & Feringa, B. L. Molecular rotary motors: Unidirectional motion around double bonds. *Proc. Natl. Acad. Sci. U.S.A.* **115**, 9423-9431 (2018).
5. Van Leeuwen, T., Lubbe, A. S., Štacko, P., Wezenberg, S. J. & Feringa, B. L. Dynamic control of function by light-driven molecular motors. *Nat. Rev. Chem.* **1**, 0096 (2017).
6. Erbas-Cakmak, S., Leigh, D. A., McTernan, C. T. & Nussbaumer, A. L. Artificial Molecular Machines. *Chem. Rev.* **115**, 10081–10206 (2015).
7. Tejeda-Rodriguez, J. A. et al. Virus‐Based Nanomotors for Cargo Delivery. *ChemNanoMat.* **5**, 194 (2019).
8. Esteban-Fernández de Ávila, B., Gao, W. W., Karshalev, E., Zhang, L. F. & Wang, J. Cell-Like Micromotors. *Acc. Chem. Res.* **51**, 1901–1910 (2018).
9. Danowski, W. et al. Unidirectional rotary motion in a metal–organic framework. *Nat. Nanotechnol.* DOI: 10.1038/s41565-019-0401-6 (2019).
10. Alam, P. et al. Spontaneous and Fast Molecular Motion at Room Temperature in the Solid State. *Angew. Chem. Int. Ed.* **58**, 4536-4540 (2018).
11. Wang, Y. P. et al. Neighboring Component Effect in a Tri-stable [2]Rotaxane. *J. Am. Chem. Soc.* **140**, 13827-13834 (2018).
12. Ma, P. X. et al. Observing the overall rocking motion of a protein in a crystal. *Nat. Commun.* **6**, 8361 (2015).
13. Zhong, D. Y. et al. Linear Alkane Polymerization on a Gold Surface. *Science* **334**, 213-216 (2011).
14. Kathan, M. et al. Light-driven molecular trap enables bidirectional manipulation of dynamic covalent systems. *Nat. Chem.***10**, 1031-1036 (2018).
15. Han, X. et al. Aggregation-induced emission behavior of a pH-controlled molecular shuttle based on a tetraphenylethene moiety. J. *Org. Biomol. Chem.* **13**, 9767-9774 (2015).
16. Cherioux, F., Galangau, O., Palmino, F. & Rapenne, G. Controlled Directional Motions of Molecular Vehicles, Rotors, and Motors: From Metallic to Silicon Surfaces, a Strategy to Operate at Higher Temperatures. *Chemphyschem.* **17**, 1742-1745 (2016).
17. Collier, C. P. et al. A [2]Catenane-Based Solid State Electronically Reconfigurable Switch. *Science* **289**, 1172-1175 (2000).
18. Song, Y., Cheng, D. & Zhao, L. *Microfluidics: Fundamentals, Devices and Applications*, Wiley-VCH Verlag GmbH & Co. KGaA: Weinheim (2018).
19. Turro, N. J., Ramamurthy, V. & Scaiano, J. C. *Modern molecular photochemistry of organic molecules*, University Science Books: Sausalito, Calif. (2010).
20. Nijegorodov, N. I. & Downey, W. S. The Influence of Planarity and Rigidity on the Absorption and Fluorescence Parameters and Intersystem Crossing Rate Constant in Aromatic Molecules. *J. Phys. Chem.* **98**, 5639–5643 (1994).
21. Birks, J. B. *Photophysics of aromatic molecules*, Wiley-Interscience: London, New York (1970).
22. Luo, J. D. et al. Aggregation-induced emission of 1-methyl-1,2,3,4,5-pentaphenylsilole. *Chem. Commun.* **0**, 1740-1741 (2001).

23. Mei, J., Leung, N. L. C., Kwok, R. T. K., Lam, J. W. Y. & Tang, B. Z. Aggregation-Induced Emission: Together We Shine, United We Soar. *Chem. Rev.* **115**, 11718-11940 (2015).
24. Liu, S. J. et al. Molecular Motion in Aggregates: Manipulating TICT for Boosting Photothermal Theranostics. *J. Am. Chem. Soc.* **141**, 5359-5368 (2019).
25. Zhang, H. et al. In situ monitoring of molecular aggregation using circular dichroism. *Nat. Commun.* **9**, 4961 (2018).
26. Dong, Y. Q. et al. Switching the light emission of (4-biphenylyl)phenyldibenzofulvene by morphological modulation: crystallization-induced emission enhancement. *Chem. Commun.* **0**, 40-42 (2007).
27. Yang, Z. et al. Recent advances in mechano-responsive luminescence of tetraphenylethylene derivatives with aggregation-induced emission properties. *Mater. Chem. Front.* **2**, 861-890 (2018).
28. Ye, R. Q. et al. Non-conventional fluorescent biogenic and synthetic polymers without aromatic rings. *Polym. Chem.* **8**, 1722-1727 (2017).
29. Gong, Y. Y. et al. Room temperature phosphorescence from natural products: Crystallization matters. *Sci. China. Chem.* **56**, 1178-1182 (2018).
30. Yuan, W. Z. & Zhang, Y. M. Nonconventional macromolecular luminogens with aggregation‐induced emission characteristics. *J. Polym. Sci. Pol. Chem.* **55**, 560-574 (2017).
31. Tomalia, D. A. et al. Non-traditional intrinsic luminescence: inexplicable blue fluorescence observed for dendrimers, macromolecules and small molecular structures lacking traditional/conventional luminophores. *Prog. Polym. Sci.* **90**, 35-117 (2019).
32. Wang, H., Zhao, E. G., Lam, J. W. Y. & Tang, B. Z. AIE luminogens: emission brightened by aggregation. *Mater. Today* **18**, 365-377 (2015).
33. Zhang, H. et al. Why Do Simple Molecules with “Isolated” Phenyl Rings Emit Visible Light? *J. Am. Chem. Soc.* **139**, 16264–16272 (2017).
34. Zhang, H. et al. Drawing a clear mechanistic picture for the aggregation-induced emission process. *Mater. Chem. Front.* DOI: 10.1039/C9QM00156E (2019).
35. Chai, J. D. & Head-Gordon, M. Long-range corrected hybrid density functionals with damped atom–atom dispersion corrections. *Phys. Chem. Chem. Phys.* **10**, 6615-6620 (2008).
36. Ruckebusch, C., Sliwa, M., Pernot, P., de Juan, A. & Tauler, R. Comprehensive data analysis of femtosecond transient absorption spectra: A review. *J. Photochem. Photobiol. C* **13**, 1-27 (2012).
37. Berera, R., van Grondelle, R. & Kennis, J. T. Ultrafast transient absorption spectroscopy: principles and application to photosynthetic systems. *Photosynth. Res.* **101**, 105-118 (2009).
38. Du, L. L., Lan, X., Yan, Z. P., Zhu, R. X. & Phillips, D. L. Time-Resolved Spectroscopic Study of N,N-Di(4-bromo)nitrenium Ions in Selected Solutions. *Molecules* **23***,* 3182 (2018).
39. Chen, X., Larsen, D. S. & Bradforth, S. E. Broadband Spectral robing Revealing Ultrafast Photochemical Branching after Ultraviolet Excitation of the Aqueous Phenolate Anion. *J. Phys. Chem. A* **115**, 3807-3819 (2011).
40. Chen, L. A. & Sung, K. Direct UV Observation and Kinetic Studies of a α-Alkoxy Benzyloxy Radical. *Org. Lett.* **11**, 3370-3373 (2009).
41. yer, E. S., Sadybekov, A., Lioubashevski, O., Krylov, A. I. & Ruhman, S. Rewriting the Story of Excimer Formation in Liquid Benzene. *J. Phys. Chem. A* **121**, 1962-1975 (2017).

42. Wang, X. H. et al. Transient Absorption Probe of Intermolecular Triplet Excimer of Naphthalene in Fluid Solutions: Identification of the Species Based on Comparison to the Intramolecular Triplet Excimers of Covalently-Linked Dimers. *J. Phys. Chem. A* **104**, 1461-1465 (2000).
43. Zhao, Z. et al. Creation of highly efficient solid emitter by decorating pyrene core with AIE-active tetraphenylethene peripheries. *Chem. Commun.* **46**, 2221-2223 (2010).
44. Ding, Y., Zhao, G., Nakai, Y. & Tsuboi, T. Temperature effect on emission spectra and fluorescence lifetime of the 4I13=2 state of Er3+-doped Gd2SiO5 crystal. *Chin. Opt. Lett.* **9**, 091602 (2011).
45. Good, H. P. The Fluorescence Lifetime of Trans‐Stilbene and its Variation with Temperature. et al. *Ber. Bunsenges. Phys. Chem.* **86**, 126-129 (1982).
46. Endo, A. et al. Thermally Activated Delayed Fluorescence from Sn4+–Porphyrin Complexes and Their Application to Organic Light Emitting Diodes — A Novel Mechanism for Electroluminescence. *Adv. Mater.* **21**, 4802-4806 (2009).
47. Tsuboi, T. & Silfsten, P. The lifetime of Eu2+ fluorescence in CaF2:Eu2+ crystals. *J. Phys. Condens. Matter.* **3**, 9163-9167 (1991).
48. Duan, C. K., Meijerink, A., Reeves, R. J. & Reid, M. F. The unusual temperature dependence of the fluorescence lifetime in crystals. *J. Alloy. Compd.* **408-412**, 784-787 (2006).
49. Liang, J.-J. et al. A blue thermally activated delayed fluorescence emitter developed by appending a fluorene moiety to a carbazole donor with meta-linkage for high-efficiency OLEDs. *Mater. Chem. Front.* **2**, 917-922 (2018).
50. Zeng, J. J. et al. Aggregation-Induced Delayed Fluorescence Luminogens for Efficient Organic Light-Emitting Diodes. *Chem. Asian J.* **14**, 828-835 (2019).
51. Atkins, P. W. & De Paula, J. *Physical chemistry for the life sciences*, Oxford University Press: Oxford (2006).
52. https://www.chem.purdue.edu/gchelp/liquids/disperse.html.